



Mn²⁺-V_{Zn}⁻ charge transfer complexes in Zn_{1-x}Mn_xTe

Le Van Khoi ^{*}, A. Avdonin , and A. Mycielski

Institute of Physics, Polish Academy of Sciences, Al. Lotnikow 32/46, 02-668 Warsaw, Poland



(Received 28 October 2022; revised 19 January 2023; accepted 13 February 2023; published 27 February 2023)

Hall effect, photoluminescence, magneto-photoluminescence, and electron paramagnetic resonance measurements performed on the undoped *p*-type ZnTe and Zn_{1-x}Mn_xTe crystals have revealed a strong coupling between Mn²⁺ ions and holes trapped at singly ionized zinc vacancy defects (V_{Zn}⁻), resulting in the formation of the Mn²⁺-V_{Zn}⁻ charge transfer complexes. These complexes cause the transformation of the 0.047 eV V_{Zn}^{-/0} shallow acceptor level, present in ZnTe, into a 0.138 eV V_{Zn}^{-/-} deep acceptor level and induce a new 1.44 eV PL band associated with Mn³⁺ ions in Zn_{1-x}Mn_xTe. The coexistence of the mixed valence Mn²⁺ and Mn³⁺ states leads to the local ferromagnetic exchange interaction between Mn²⁺ and Mn³⁺ ions. The competition between the ferromagnetic exchange interaction and the intrinsic Mn²⁺-Mn²⁺ antiferromagnetic superexchange coupling gives rise to the paramagnetic–spin glass phase transition at $T_f = 3.2$ K in the Zn_{1-x}Mn_xTe samples with $x = 0.06$. We suggest a charge transfer mechanism, which transforms the Mn²⁺-V_{Zn}⁻ complexes into Mn³⁺-V_{Zn}⁻ ones. The effect of Mn²⁺ on the *p*-type doping of the II-VI compounds is discussed.

DOI: [10.1103/PhysRevB.107.085206](https://doi.org/10.1103/PhysRevB.107.085206)

I. INTRODUCTION

Dilute magnetic semiconductors (DMSs) of the A_{1-x}B_x type have been the subject of intense research for more than four decades, both because of the fundamental interest and because of the promise they hold for spin-based electronic devices. Among the A_{1-x}B_x DMSs the bulk Zn_{1-x}Mn_xTe is very interesting because it is the only alloy which has a *p*-type electrical conductivity and a band gap energy E_g higher than the energy of the Mn²⁺ intrashell transitions [1]. Because of these properties, the exciton and donor-acceptor-pair (DAP) photoluminescence (PL) from the bulk Zn_{1-x}Mn_xTe do not suffer from the PL quenching effect usually observed in *n*-type DMSs. Therefore, these near-band-edge emissions can be studied in parallel with the Mn-related emission, even in a low-*x* limit. This provides an opportunity to optically study the exchange coupling between individual Mn²⁺ ions and paramagnetic deep level defects, such as zinc vacancies V_{Zn} in the bulk Zn_{1-x}Mn_xTe crystals.

Recently, we have reported that doping Zn_{1-x}Mn_xTe with phosphorus (P) acceptor impurity can change the charge state of Mn ions from Mn²⁺ to Mn³⁺ [2]. Therefore, it is useful to examine whether the intrinsic acceptor defects such as zinc vacancies V_{Zn} can also have an effect on the charge state of Mn.

It is established that in ZnTe the main intrinsic point defects are the V_{Zn} which can exist in three charge states: neutral V_{Zn}⁰, singly negatively charged V_{Zn}⁻, and doubly negatively charged V_{Zn}^{-/-}. These charge states introduce two (V_{Zn}^{-/0}) and (V_{Zn}^{-/-}) energy levels into the band gap [3]. The isolated V_{Zn}⁻ defect is stable at room temperature and is paramagnetic [4,5]. The incorporation of Mn atoms into the ZnTe host may cause

strong *p-d* interactions between the Mn²⁺ ions and holes trapped at the V_{Zn}⁻ acceptors. This coupling may give rise to the formation of the Mn²⁺-V_{Zn}⁻ complexes which strongly impact on the transport, optical, and magnetic properties in the undoped Zn_{1-x}Mn_xTe DMS.

Also, in Zn_{1-x}Mn_xTe the energy of the Mn²⁺ intrashell transitions (≈ 2.0 eV) is smaller than that of the donor-deep acceptor pair (DAP) transition (≈ 2.21 eV). Therefore, the selective excitation of the DAP transition, i.e., the below-band-gap excitation, may induce the emission associated with Mn internal transitions. This may provide a new way for the optical excitation of the Mn ions in the absence of band carriers.

In this paper we employ the results of Hall effect, PL, magneto-PL, and electron paramagnetic resonance (EPR) measurements of undoped *p*-type ZnTe and Zn_{1-x}Mn_xTe crystals to bring the evidence of a strong interaction between Mn²⁺ ions and singly charged zinc vacancy defects, Mn²⁺-V_{Zn}⁻, which involves a charge transfer between them and formation of complex defects Mn³⁺-V_{Zn}^{-/-}. In experiments, this charge transfer is manifested in the disappearance of the 47 meV V_{Zn}^{-/0} shallow acceptor, present in ZnTe, and the appearance of a 138 meV V_{Zn}^{-/-} deep acceptor level, and in the appearance of a new PL band at 1.44 eV, associated with Mn³⁺ ions in Zn_{1-x}Mn_xTe. Manganese ions which remain not associated with any zinc vacancy are in the charge state Mn²⁺. The coexistence of the mixed valence states of Mn²⁺ and Mn³⁺ ions leads to ferromagnetic double-exchange interaction between manganese ions. The competition between the ferromagnetic double-exchange and the antiferromagnetic superexchange interactions is seen in EPR experiments as a transition from paramagnetic to spin-glass phase at $T_f = 3.2$ K in Zn_{1-x}Mn_xTe samples with $x = 0.06$. In the following, the effect of Mn²⁺ on the *p*-type doping of the II-VI compounds is discussed.

*lkhoi@ifpan.edu.pl

Our paper is organized as follows. Section II describes the sample preparation and experimental methods. Section III is divided into three subsections. In Sec. III A the temperature dependencies of the free hole concentration and hole ionization energies are determined. The formation of the charge transfer state for Mn^{2+} ions is proposed. In Sec. III B the PL and magneto-PL results are presented and discussed. The main point of this part is the identification of the emission related to the Mn^{3+} ions. In Sec. III C results of the EPR measurements are reported. The magnetic susceptibility of $\text{Zn}_{1-x}\text{Mn}_x\text{Te}$ is determined. Section IV contains the discussion in which we report that the compensation of the acceptor impurities by Mn^{2+} ions is a common property in the Mn-based DMS. The paper is concluded by a summary.

II. SAMPLE PREPARATION AND EXPERIMENTAL METHODS

$\text{Zn}_{1-x}\text{Mn}_x\text{Te}$ crystals were grown at 1595 K by the high-pressure Bridgman method from $(\text{ZnTe})_{1-x}(\text{MnTe})_x$ solution in an evacuated (10^{-6} Torr) quartz ampoule coated with pyrolytic graphite. ZnTe and MnTe polycrystal sources were synthesized from 6N purity Zn, Mn, Te elements and weighted to reach the desired stoichiometric ratio for a nominal Mn molar content x_n . Because of high crystallization temperature and high partial pressure of Zn, the undoped ZnTe and $\text{Zn}_{1-x}\text{Mn}_x\text{Te}$ crystals have a large number of native Zn-vacancy defects V_{Zn} . The ZnTe and $\text{Zn}_{1-x}\text{Mn}_x\text{Te}$ samples split from the as-grown ingot were additionally subjected to annealing at 1100 K and pressure of 4 MPa of nitrogen gas to improve the composition homogeneity.

The actual Mn content x in each sample was determined by the energy dispersive x-ray fluorescence analysis (EDXFA). The EDXFA measurements were carried out at 300 K using the Spectrace 5000 Tracor Xray spectrometer equipped with a Si (Li) detector.

Resistivity and Hall effect measurements were performed on bar-shaped samples with six gold contacts. The sample dimensions were $8 \times 1.5 \times 0.5 \text{ mm}^3$. The measurements were performed between room temperature and 100 K. The Hall voltage was measured by a Keithley nanovoltmeter model 2182A. The sample temperature is controlled by a continuous-flow cryostat equipped with a temperature controller LakeShore 332. A resistive magnet which can deliver maximum magnetic field of 1.5 T was used. The dc currents between 0.1 nA and 10 mA have been provided by a Keithley current source model K220.

Electron paramagnetic resonance (EPR) experiments were carried out using a Bruker ESP-300 X-band spectrometer with 100 Hz field modulation and phase-sensitive detection, which operated at a microwave frequency of about 9.4 MHz. The magnetic field was applied in the [110] crystal plane. The sample temperature is controlled by a continuous He gas flow Oxford Instruments cryostat.

Photoluminescence experiments were performed on $\text{Zn}_{1-x}\text{Mn}_x\text{Te}$ freshly cleaved crystals. The PL signal was excited using two laser diodes: at 561 nm (Cobolt Jive 561) or 488 nm (Omicron LuxX 488). Both laser beams were delivered using the same single-mode fiber, which allowed us to seamlessly change the excitation wavelength

TABLE I. Characteristics of the investigated samples of $\text{Zn}_{1-x}\text{Mn}_x\text{Te}$. Quantities: x is the Mn molar fraction, p is the free hole concentration determined from the Hall effect measurement, PL and R denote the photoluminescence and reflection measurements.

Sample	x	Measurements	p (300 K) (m^{-3})
ZnTe	0	PL, R, Hall effect	2.8×10^{22}
$\text{Zn}_{0.999}\text{Mn}_{0.001}\text{Te}$	0.001	PL, R, Hall effect	7.56×10^{21}
$\text{Zn}_{0.985}\text{Mn}_{0.015}\text{Te}$	0.015	PL, R	
$\text{Zn}_{0.97}\text{Mn}_{0.03}\text{Te}$	0.03	PL, R, EPR, Hall effect	1.1×10^{22}
$\text{Zn}_{0.96}\text{Mn}_{0.04}\text{Te}$	0.04	PL, magneto-PL	
$\text{Zn}_{0.94}\text{Mn}_{0.06}\text{Te}$	0.06	Magneto-PL, EPR	

without changing the spot on the sample. The PL signal was resolved using a 500 mm spectrometer (Andor Shamrock 500) and recorded using a CCD camera (Andor Newton). For magneto-PL measurements a superconducting-magnet liquid helium cryostat (SpectroMag Oxford Instruments) capable of generating magnetic fields up to 10 T as well as temperatures below 2 K was used.

Optical reflectivity measurements were carried out in Faraday geometry. The incident light was provided by a high-pressure Xe lamp and directed nearly perpendicular to cleaved (110) surfaces of $\text{Zn}_{1-x}\text{Mn}_x\text{Te}$ crystals.

Table I presents a list of the $\text{Zn}_{1-x}\text{Mn}_x\text{Te}$ samples and their characteristics.

III. EXPERIMENTAL RESULTS AND ANALYSIS

A. Zinc vacancy defect levels

Hall effect measurements performed at 300 K for the ZnTe and $\text{Zn}_{1-x}\text{Mn}_x\text{Te}$ crystals have shown that these crystals exhibit a p -type electrical conductivity due to the native V_{Zn} zinc vacancy defects and are highly compensated. The temperature dependence of free hole concentration (p) has been measured in the temperature range 100–300 K and analyzed using expression (1) for the compensated p -type semiconductor in which concentration p in the valence band is smaller than that of the compensating donor $p \ll N_D$ and $p \ll N_A - N_D$ [6],

$$p = \frac{N_V}{4} \left(\frac{1}{k} - 1 \right) \exp \left(-\frac{E_A}{k_B T} \right), \quad (1)$$

where $k = N_D/N_A$ is the degree of compensation of acceptors by donors, N_D and N_A are the residual donor and zinc vacancy acceptor concentrations, respectively, $N_V = 2(2\pi m_v^* k_B T / h^2)^{3/2}$ is the effective density of states in the valence band, E_A is the acceptor ionization energy, k_B is the Boltzmann constant, h is the Planck constant, and m_v is the density-of-states mass.

Figure 1(a) presents the temperature dependence of hole concentration for ZnTe, $\text{Zn}_{0.999}\text{Mn}_{0.001}\text{Te}$, and $\text{Zn}_{0.97}\text{Mn}_{0.03}\text{Te}$. Three features can be seen in this figure:

(a1) At 300 K, the hole concentration in ZnTe ($p = 2.8 \times 10^{22} \text{ m}^{-3}$) has the same order of magnitude as in $\text{Zn}_{0.999}\text{Mn}_{0.001}\text{Te}$ or $\text{Zn}_{0.97}\text{Mn}_{0.03}\text{Te}$ ($p = 1 \times 10^{22} \text{ m}^{-3}$).

(a2) As the sample temperature is decreased from 300 K to 100 K, the hole concentration in ZnTe decreases by a factor

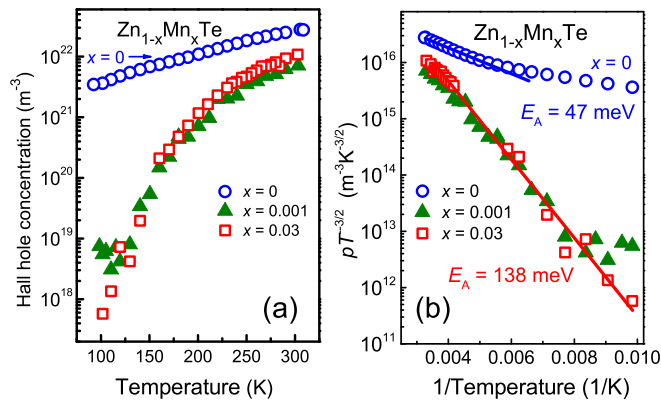


FIG. 1. (a) Temperature dependence of free hole concentration (p) measured in the temperature range 100–300 K for ZnTe (blue circles), $\text{Zn}_{0.999}\text{Mn}_{0.001}\text{Te}$ (olive up-triangles), and $\text{Zn}_{0.97}\text{Mn}_{0.03}\text{Te}$ (red squares). (b) Plots of $pT^{-3/2}$ versus $1/T$ (symbols) for the same samples as in (a). Solid lines represent the linear fits which serve us to determine the acceptor ionization energy.

of 3, whereas the hole concentration in $\text{Zn}_{0.999}\text{Mn}_{0.001}\text{Te}$ and $\text{Zn}_{0.97}\text{Mn}_{0.03}\text{Te}$ decreases by about 4 orders of magnitude.

(a3) Despite the fact that the Mn fraction x in $\text{Zn}_{0.97}\text{Mn}_{0.03}\text{Te}$ is greater than that in $\text{Zn}_{0.999}\text{Mn}_{0.001}\text{Te}$ by a factor of 30, the values of the hole concentrations in both samples are practically equal.

In order to determine the ionization energies E_A of the V_{Zn} double acceptors, we present in Fig. 1(b) plots of $(pT^{-3/2})$ versus $1/T$ (symbols) along with the linear fits (solid lines) for samples ZnTe, $\text{Zn}_{0.999}\text{Mn}_{0.001}\text{Te}$, and $\text{Zn}_{0.97}\text{Mn}_{0.03}\text{Te}$ in the temperature range 100–300 K. E_A is determined from the slope of the fitted lines. We have found that $E_A^1 = 0.047 \pm 0.002$ eV for ZnTe, and $E_A^2 = 0.138 \pm 0.002$ eV for $\text{Zn}_{0.999}\text{Mn}_{0.001}\text{Te}$ or $\text{Zn}_{0.97}\text{Mn}_{0.03}\text{Te}$. The value $E_A^1 = 0.047$ eV is close to the reported ionization energy (0.048 eV) of the V_{Zn}^- shallow acceptors, while the values $E_A^2 = 0.138$ eV are close to the calculated ionization energy (0.140 eV) of the V_{Zn}^{--} deep acceptors in ZnTe [3,7].

Taking the value of the heavy-hole effective mass $m_{hh}^* = 0.60m_0$ [8], the localization radius ($a_l = \hbar/\sqrt{2m_{hh}^*E_A}$) for the hole trapped at the V_{Zn}^0 neutral and V_{Zn}^- singly ionized acceptors are equal to 11 Å and 6.7 Å, respectively.

Knowing the positions of the energy levels associated with the V_{Zn} defects in ZnTe, and in $\text{Zn}_{0.999}\text{Mn}_{0.001}\text{Te}$ and $\text{Zn}_{0.97}\text{Mn}_{0.03}\text{Te}$ samples, we can make the following conclusions from the mentioned above features.

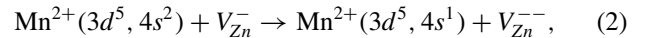
Feature (a1) shows that concentrations of the V_{Zn} acceptors are nearly equal in samples ZnTe, $\text{Zn}_{0.999}\text{Mn}_{0.001}\text{Te}$, and $\text{Zn}_{0.97}\text{Mn}_{0.03}\text{Te}$, because at 300 K the hole concentrations are comparable.

Feature (a2) shows that the hole concentration in ZnTe is determined by the 0.047 eV $V_{\text{Zn}}^{-/0}$ shallow level, whereas in $\text{Zn}_{0.999}\text{Mn}_{0.001}\text{Te}$ and $\text{Zn}_{0.97}\text{Mn}_{0.03}\text{Te}$ the hole concentration is determined by the 0.138 eV $V_{\text{Zn}}^{--/}$ deep level. This can be viewed as transformation of the 0.047 eV shallow level, presented in ZnTe, into a new 0.138 eV deep level in $\text{Zn}_{0.999}\text{Mn}_{0.001}\text{Te}$ or in $\text{Zn}_{0.97}\text{Mn}_{0.03}\text{Te}$. The shallow to deep level transformation in $\text{Zn}_{0.999}\text{Mn}_{0.001}\text{Te}$ or in $\text{Zn}_{0.97}\text{Mn}_{0.03}\text{Te}$ must be due to the presence of Mn. This fact indicates that

the incorporated Mn^{2+} ions strongly couple with the V_{Zn}^- acceptors. That gives rise to the formation of the $\text{Mn}^{2+}-V_{\text{Zn}}^-$ complexes.

Feature (a3) indicates that in $\text{Zn}_{0.999}\text{Mn}_{0.001}\text{Te}$ or $\text{Zn}_{0.97}\text{Mn}_{0.03}\text{Te}$ the individual Mn^{2+} ions not pairing with V_{Zn}^- acceptors are electrically inactive.

In order to explain how the formation of the $\text{Mn}^{2+}-V_{\text{Zn}}^-$ complexes leads to the transformation of the 0.047 eV $V_{\text{Zn}}^{-/0}$ shallow acceptor's level into the 0.138 eV $V_{\text{Zn}}^{--/}$ deep level, we notice that (i) the localization radius $a_l = 6.7$ Å of the holes trapped at the V_{Zn}^- acceptors is very close to the lattice constant $a = 6.102$ Å of ZnTe; i.e., these holes are strongly localized. (ii) In ZnTe the hole trapped at the V_{Zn}^- defect tends to localize on only one of four Te neighbors and it can “hop” between four Te neighbors to find the lowest energy position [9,10]. Therefore, we suggest that the $\text{Mn}^{2+}-V_{\text{Zn}}^-$ coupling makes one of the Mn $4s^2$ bonding electrons hop to the vacant place of the V_{Zn}^- site leaving a $4s$ hole tightly bound to the Mn^{2+} site, and creating the V_{Zn}^{--} charge state. This transition can be described by



where $4s^2$ and $4s^1$ denote the number of the s electrons of Mn contributed to the covalence bonds with Te neighbors. It is seen that transition (2) gives rise to the change of the charge state of the V_{Zn}^- site from -1 to -2 . In consequence the 0.47 eV $V_{\text{Zn}}^{-/0}$ level connected with the V_{Zn}^- acceptors is compensated. As shown below in Sec. III B, the PL measurements have revealed an emission band at 1.44 eV from the $\text{Zn}_{1-x}\text{Mn}_x\text{Te}$ crystals which is attributed to the Mn^{3+} ions. This finding indicates that the $4s$ -bonding hole favors entering the d shell to be delocalized among the Mn^{3+} and Mn^{2+} ions by the double-exchange mechanism [11]. Therefore, transition (2) can be continued as



Transitions (2) and (3) show that the $\text{Mn}^{2+}-V_{\text{Zn}}^-$ exchange coupling gives rise to the charge transfer between Mn^{2+} ions and V_{Zn}^- acceptor defects that results in the formation of the $\text{Mn}^{3+}-V_{\text{Zn}}^{--}$ complexes. This means that the V_{Zn}^- acceptor is compensated by the Mn^{2+} ion.

It is worth noting that the compensation of the V_{Zn}^- acceptors in ZnTe was previously observed in the case of the doping of ZnTe with Cu, Ag, Au impurities [3,12]. In Ref. [3] the authors reported that doping ZnTe with the Cu impurity leads to the disappearance of the 0.048 eV shallow level and the appearance of the 0.150 eV deep level. They suggested that Cu ions can pair with the V_{Zn}^- vacancies and act as donors.

Summarizing this subsection, the ionization energies of the V_{Zn}^- shallow acceptors in ZnTe and of the V_{Zn}^{--} deep acceptors in $\text{Zn}_{1-x}\text{Mn}_x\text{Te}$ have been determined. The $\text{Mn}^{2+}-V_{\text{Zn}}^-$ coupling gives rise to the formation of the $\text{Mn}^{2+}-V_{\text{Zn}}^-$ complexes. We suggest a charge transfer mechanism which transforms the $\text{Mn}^{2+}-V_{\text{Zn}}^-$ complexes into the $\text{Mn}^{3+}-V_{\text{Zn}}^{--}$ ones.

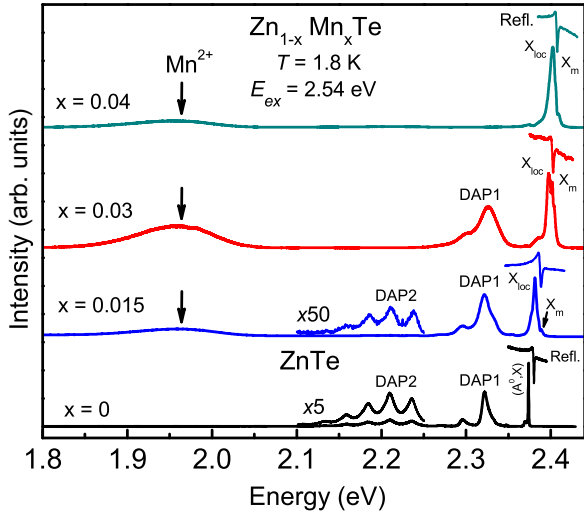
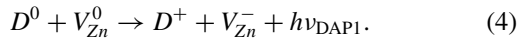


FIG. 2. Photoluminescence and optical reflection spectra measured at 1.8 K and under the 2.54 eV excitation of ZnTe and $\text{Zn}_{1-x}\text{Mn}_x\text{Te}$ with $x = 0.015, 0.03,$ and 0.04 . X_m and X_{loc} denote the emission lines due to mobile excitons and localized excitons. (A^0, X) is the emission line due to the excitons bound to neutral acceptors. DAP1 and DAP2 designate the emission bands resulting from the transitions of electrons from the residual donor ($D^{0/+}$) level to the shallow ($V_{\text{Zn}}^{-/0}$) and deep ($V_{\text{Zn}}^{--/-}$) acceptor levels, respectively. Mn^{2+} denotes the emission band associated with the Mn^{2+} intrashell transitions. The optical reflection spectra (labeled “Refl.”) were measured on the same samples which were used for the PL experiments and serve us to determine the free exciton energies.

B. Photoluminescence due to Mn^{2+} and Mn^{3+}

A fortunate feature of ZnTe and $\text{Zn}_{1-x}\text{Mn}_x\text{Te}$ is that the V_{Zn} defects are active not only electrically but also optically; therefore, we can probe the presence of the $\text{Mn}^{3+}-V_{\text{Zn}}^{--}$ complexes by the PL spectroscopy and study their effects on the PL properties in $\text{Zn}_{1-x}\text{Mn}_x\text{Te}$.

Figure 2 presents the PL and reflection spectra measured at 1.7 K under the 2.54 eV laser excitation for $\text{Zn}_{1-x}\text{Mn}_x\text{Te}$ with $x = 0.015, 0.03,$ and 0.04 , and for ZnTe as a reference specimen. The reflection spectrum of the ZnTe sample shows a free exciton resonance at $E_X = 2.380 \pm 0.01$ eV. The PL spectrum of the ZnTe sample consists of three PL bands. Beginning with high energies, the first band at 2.374 eV is attributed to the recombination of excitons bound to neutral acceptors [labeled (A^0, X)]. In this case the neutral acceptors are the neutral Zn vacancies V_{Zn}^0 [13]. The second band at 2.323 eV (labeled DAP1) is due to the recombination of the electrons bound to the residual neutral donors (D^0) with the holes trapped at the V_{Zn}^0 neutral acceptors (called the DAP1 transition). This DAP1 transition can be represented by the reaction



The third band at 2.236 eV (labeled DAP2) and its strong phonon replicas are assigned to the recombination of the electrons bound to the D^0 donors with the holes trapped at the V_{Zn}^- singly ionized acceptors [7] (called the DAP2 transition). This

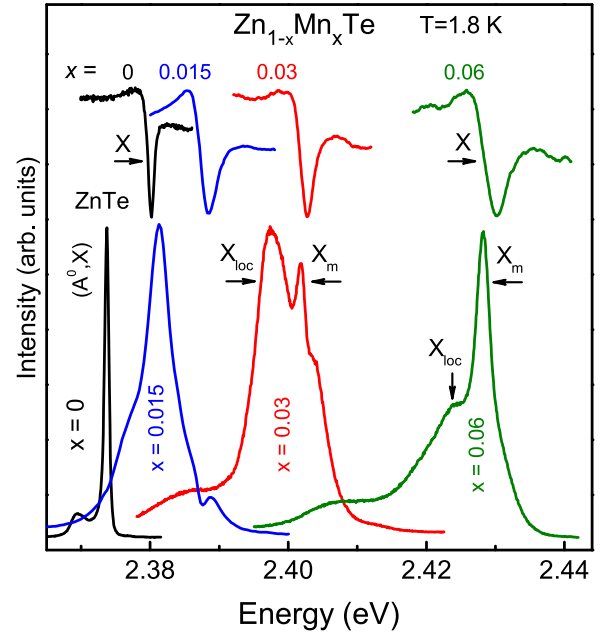
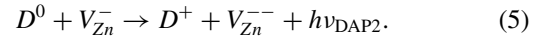


FIG. 3. Evolution of the exciton photoluminescence and optical reflection spectra with Mn content x for $\text{Zn}_{1-x}\text{Mn}_x\text{Te}$ with $x = 0, 0.015, 0.03,$ and 0.06 . The labels have the same meaning as in Fig. 2. Note that the X_{loc} line originating from the (A^0, X) line of ZnTe is suppressed in the PL spectrum of $\text{Zn}_{0.94}\text{Mn}_{0.06}\text{Te}$.

DAP2 transition can be represented by the reaction



The donor impurity D^+ may be Cl_{Te}^+ or Al_{Zn}^+ [14].

The PL spectra of $\text{Zn}_{1-x}\text{Mn}_x\text{Te}$ samples exhibit four new features due to the presence of Mn, in comparison with the PL spectrum of the ZnTe reference sample.

(b1) The exciton emission band is broadened and consists of two lines which are assigned to the recombination of the excitons localized by the alloy potential fluctuation X_{loc} and mobile excitons X_m [15]. The intensities of these lines are strongly dependent on Mn composition. This effect will be demonstrated in Fig. 3 and analyzed in more detail below.

(b2) The DAP1 band displayed in the PL spectra of ZnTe, $\text{Zn}_{0.985}\text{Mn}_{0.015}\text{Te}$, and $\text{Zn}_{0.97}\text{Mn}_{0.03}\text{Te}$ is suppressed in the PL spectrum of $\text{Zn}_{0.96}\text{Mn}_{0.04}\text{Te}$. We have observed that for $x \geq 0.04$ the PL spectrum of $\text{Zn}_{1-x}\text{Mn}_x\text{Te}$ excited by the 2.54 eV excitation exhibits only the excitonic and Mn^{2+} emission bands.

(b3) The third is the decrease in the intensity of the DAP2 band in the PL spectrum of $\text{Zn}_{0.985}\text{Mn}_{0.015}\text{Te}$ by a factor of 10 in comparison with the intensity of the DAP2 band in the PL spectrum of ZnTe, and the complete quenching of this DAP2 band in the PL spectrum of $\text{Zn}_{0.97}\text{Mn}_{0.03}\text{Te}$ and $\text{Zn}_{0.96}\text{Mn}_{0.04}\text{Te}$.

(b4) The fourth is the appearance of a new PL band associated with Mn ions at 1.964 eV (labeled Mn^{2+}) in all samples of $\text{Zn}_{1-x}\text{Mn}_x\text{Te}$. The spectral position of this band is independent from Mn content x [see Fig. 4(b)]. This band is attributed to the Mn^{2+} intrashell spin forbidden transition ${}^4T_1 \rightarrow {}^6A_1$ [16–19].

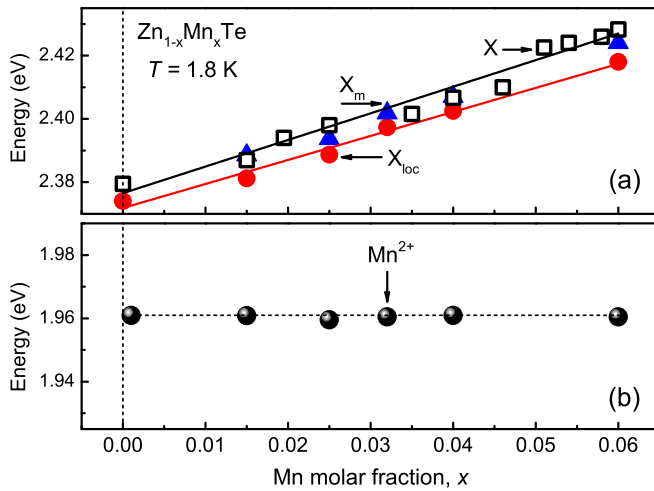


FIG. 4. Composition dependence of the energy of (a) the free exciton (squares), mobile (blue triangles), and localized (red circles) PL excitons and (b) Mn²⁺ PL emissions.

Because we are interested in the interaction of individual Mn²⁺ ions with V_{Zn}⁻ acceptors which are responsible for the DAP1 and DAP2 PL band [see reaction (5)], we first focus on features (b2) and (b3). We interpret these features by the coupling of Mn²⁺ ions with V_{Zn}⁻ acceptors which gives rise to the formation of the positively charged (Mn³⁺-V_{Zn}⁻)⁺ complexes, as discussed in Sec. III A. Under the above band gap (2.54 eV) excitation these positively charged complexes cannot trap the photoexcited holes; i.e., the V_{Zn}⁻ acceptors become optically inactive by coupling with Mn²⁺ ions. This causes the suppression of the DAP2 PL band in Zn_{1-x}Mn_xTe. We consider the quenching of the DAP2 PL band as the optical indication of the presence of Mn³⁺ - V_{Zn}⁻ complexes in Zn_{1-x}Mn_xTe.

Because the V_{Zn}⁰ neutral acceptors can be described as V_{Zn}⁰ ≡ V_{Zn}⁻ + h⁺, where h⁺ denotes the photogenerated hole trapped at V_{Zn}⁻ acceptor, the Mn²⁺-V_{Zn}⁻ coupling inducing the transformation of V_{Zn}⁻ acceptors to V_{Zn}⁻ ones should give rise to decrease in the concentration of the V_{Zn}⁰ photoexcited neutral acceptors. In consequence, the DAP1 PL band resulting from transition (4) should be quenched. In fact, the PL spectrum for the Zn_{0.96}Mn_{0.04}Te sample presented in Fig. 2 shows that the DAP1 PL band is quenched. The DAP1 band presented in the PL spectra of Zn_{0.985}Mn_{0.015}Te and Zn_{0.97}Mn_{0.03}Te in Fig. 2 is due to the inhomogeneities caused by the Mn composition fluctuation. That leads to the existence of the alloy regions where the Mn²⁺ ions were poorly incorporated. From these alloy regions the DAP1 emission may occur.

In order to demonstrate the effects of Mn content on the spectral position of the free exciton resonances X of the optical reflection spectra and on the intensities of the X_{loc} and X_m PL lines we present in Fig. 3 the reflection spectra and fragments of the exciton PL from the full-scale PL spectra shown in Fig. 2 for ZnTe and Zn_{1-x}Mn_xTe with x = 0.015, 0.03 and 0.06. One can see that the excitonic PL spectrum of ZnTe exhibits only one narrow (A⁰, X) line with a linewidth of ~2 meV, whereas in the PL spectra of Zn_{1-x}Mn_xTe this (A⁰, X) line is broadened due to Mn²⁺-V_{Zn}⁻ coupling and alloy compositional fluctuation. We rename this (A⁰, X) line as the localized exciton line X_{loc}. We have observed that

in Zn_{1-x}Mn_xTe samples with x ≥ 0.03 a new emission line appears at an energy nearly equal to the energy of the free excitons determined from the reflection spectrum. We attribute this new line to the recombination of mobile excitons and denote it as X_m. The peak intensity of the X_m line is comparable with that of the X_{loc} line. For the Zn_{1-x}Mn_xTe sample with higher Mn fraction x = 0.06 the X_{loc} line is practically suppressed and the X_m line dominates the PL spectrum. We explain the suppression of the X_{loc} line by the Mn²⁺-V_{Zn}⁻ coupling which transforms all the V_{Zn}⁻ acceptors into V_{Zn}⁻ ones. That shows that the neutral acceptors V_{Zn}⁰ ≡ V_{Zn}⁻ + h⁺ acting as trapping centers for the photogenerated excitons cease to exist. In consequence, the photogenerated excitons remain mobile and their recombination results in the X_m emission band which dominates the exciton PL spectrum.

Figure 4(a) presents the composition dependence of the energy E_X of the free excitons determined from the spectral positions of the reflection spectra, and peak energies E_{loc} and E_m of the X_{loc} and X_m PL lines, respectively. We have observed that the dependence of E_X and E_m on Mn content can be expressed as

$$E = (2.380 \pm 0.002) + 0.661x \text{ [eV]}. \quad (6)$$

This result shows that the free excitons detected in the optical reflection experiment and mobile excitons detected in the PL measurements should have the same origin. Figure 4(b) presents the dependence of the peak energy E_{Mn} of the Mn²⁺ emission on Mn content. It is seen that E_{Mn} ≈ 1.96 eV is independent of molar fraction of Mn. The pinning of the emission energy at 1.96 eV implies that the recombination transitions responsible for the Mn emission occur within the 3d levels, ⁴T₁ → ⁶A₁.

It is worth noticing that, at first look, one may think that the suppression of the DAP2 band may be caused by the Auger-like recombination with the energy transfer from the DAP2 transition [see reaction (5)] to Mn²⁺ ions that should lead to the occurrence of the Mn²⁺ PL band. The excitation mechanism of Mn²⁺ ions in Zn_{1-x}Mn_xTe is similar to that of the Auger recombination of the band carriers, with the excitation of Mn²⁺ ions in Cd_{1-x}Mn_xS [20]. If this energy transfer mechanism of Mn excitation is realized, then under application of an external magnetic field the intensity of the Mn²⁺ emission should be decreased due to the polarization of Mn²⁺ ions and band carriers [16,20].

However, our study of the PL properties in Zn_{1-x}Mn_xTe in the presence of magnetic field [1] shows that the PL emission from Mn²⁺ gains in intensity with increasing magnetic field. Moreover, the Mn²⁺ emission becomes spin-polarized. It develops a negative circular polarization (CP_{Mn}) of ~-14%. The behavior of the Mn²⁺ emission in magnetic field points to the absence of the energy transfer from the exciton or DAP transitions to Mn²⁺ ions in Zn_{1-x}Mn_xTe. This fact supports the above conclusion that the suppression of the DAP2 PL band is due to the formation of the Mn³⁺-V_{Zn}⁻ complexes in Zn_{1-x}Mn_xTe.

Looking for the PL signature of the Mn³⁺ ions we have found that when we decrease the laser excitation energy E_{ex} from 2.541 eV (above band gap excitation) to 2.211 eV (below band gap excitation) the intensity of the Mn²⁺ emission increases by 50 times and a new PL emission band at

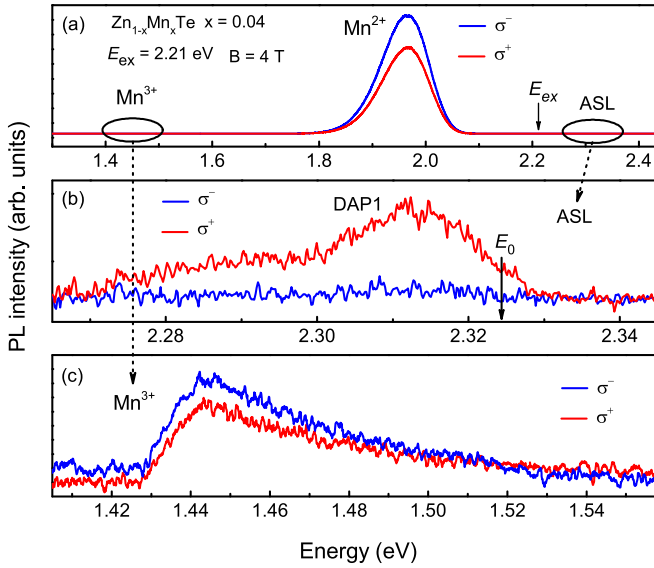


FIG. 5. (a) Mn^{2+} photoluminescence spectra excited at 2.21 eV (below band gap excitation), and measured at $T = 1.8$ K and $B = 4$ T for $Zn_{0.96}Mn_{0.04}Te$. (b) Magnified 2.32 eV anti-Stokes (ASL) band. E_0 marks the energy of the DAP1 band at $B = 0$ T. (c) Magnified 1.44 eV PL band from Mn^{3+} ions.

1.44 eV emerges at the same time. The excitation energy $E_{ex} = 2.211$ eV is very close to the peak energy of the DAP2 band (2.214 eV); i.e., this excitation is in resonance with the DAP2 transition. The exact electronic mechanism responsible for the increase of the Mn^{2+} emission intensity is not clear at present, but we suggest that the increase of the penetration depth of the 2.211 eV laser beam may cause more individual Mn^{2+} ions to take part in the excitation and recombination processes.

Figure 5(a) presents the σ^+ and σ^- polarized PL spectra measured with the 2.211 eV excitation for the spectral range from 1.30 to 2.44 eV and at $B = 4$ T for $Zn_{0.96}Mn_{0.04}Te$ sample. These spectra consist of three emission bands. Beginning from high energies, (1) the weak PL band at 2.313 eV is due to anti-Stokes luminescence (labeled ASL). The energy of this ASL band is higher than the excitation energy by 0.11 eV. The ASL band is magnified and displayed in Fig. 4(b). (2) The strong PL band at 1.96 eV is due to Mn^{2+} ions (labeled Mn^{2+}). (3) The third is the new PL band at 1.44 eV (labeled Mn^{3+}) which is magnified and displayed in Fig. 4(c). The peak energy of the ASL band is close to the peak energy (2.323 eV) of the DAP1 band. Therefore, the ASL band is attributed to the DAP1 recombination transition. The spin-polarized emission due to Mn^{2+} ions in the presence of magnetic field has been discussed in our previous paper [1] and in Refs. [16,21].

We explain the appearance of the new 1.44 eV PL band, occurring under the DAP2 resonant excitation, by the Auger-type DAP2 recombination with energy transfer to Mn^{3+} ions of the $Mn^{3+} + V_{Zn}^-$ complexes. It is noticed that the intra- Mn^{3+} transitions ${}^5T_2 \rightarrow {}^5E$ are spin allowed in a cubic crystal field [22]. Therefore, the energy transfer from the DAP2 recombination events can excite the Mn^{3+} ions and make the DAP2 transition nonradiative. The intra- Mn^{3+} recombination

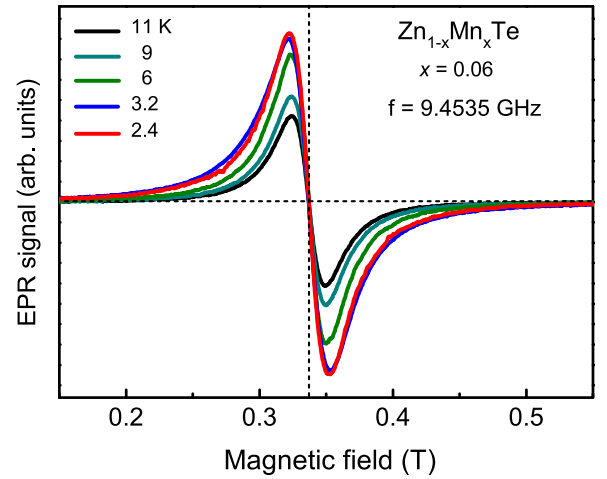


FIG. 6. X-band EPR spectra measured at various temperatures for $Zn_{0.94}Mn_{0.06}Te$.

transitions results in the 1.44 eV PL band. This conclusion is supported by the fact that the peak energy (1.44 eV) of the new PL band is close to the energy of the Mn^{3+} PL band (1.423 eV) from the GaN:Mn epitaxial layer grown on the Si(111) substrate [23], and from the bulk GaN:(Mn,Mg) (1.41 eV) [24] and $Zn_{1-x}Mn_xTe:P$ (1.49 eV) [2] crystals.

The detection of both emissions from Mn^{2+} and Mn^{3+} ions in parallel indicates the presence of the individual Mn^{2+} ions and the Mn^{2+} ions coupled with V_{Zn}^- defects, which results in the $Mn^{3+}-V_{Zn}^-$ complexes. The revealing of PL emission from Mn^{3+} ions is an important experimental fact which supports the charge transfer mechanism represented by transitions (2) and (3) in Sec. III A for the $Mn^{2+}-V_{Zn}^-$ complexes.

It is interesting to notice that the quenching of the DAP2 band due to the $Mn^{2+}-V_{Zn}^-$ coupling in $Zn_{1-x}Mn_xTe$ [feature (b3)] has also been observed in the case of the CdTe crystals doped with chromium (Cr) and vanadium (V) atoms [25]. The authors of Ref. [25] have observed that the introduction of the Cr^{2+} impurity into the CdTe compound causes a strong quenching of the 1.42 eV (DAP2) PL emission associated with the singly charged cadmium vacancy defects, V_{Cd}^- . Therefore, the suppression of the DAP2 PL band in $Zn_{1-x}Mn_xTe$ and in CdTe:(Cr,V), due to the transition metal (TM) impurities, indicates that the charge transfer between the substitutional TM ions and the V_{Zn}^- or V_{Cd}^- defects is a common property for $Zn_{1-x}Mn_xTe$ and CdTe:(Cr,V) DMSs. This property is caused by the similarity of the electronic structures of the V_{Zn}^- or V_{Cd}^- defects which are formed by four Te dangling bonds [9,26].

C. Magnetic susceptibility

The $Mn^{2+}-V_{Zn}^-$ coupling results in Mn^{3+} ions and V_{Zn}^- acceptors. The resulting coexistence of the mixed valence Mn^{2+} and Mn^{3+} ions strongly affects the magnetic properties in $Zn_{1-x}Mn_xTe$ which can be analyzed from the variation of the intensity of the EPR signal with temperature.

Figure 6 presents the EPR spectra measured at various temperatures below 12 K for the $Zn_{0.94}Mn_{0.06}Te$ sample. The spectrum consists of a single resonance line which is characterized by a g factor $g = 2.0048 \pm 0.0005$. We assign this

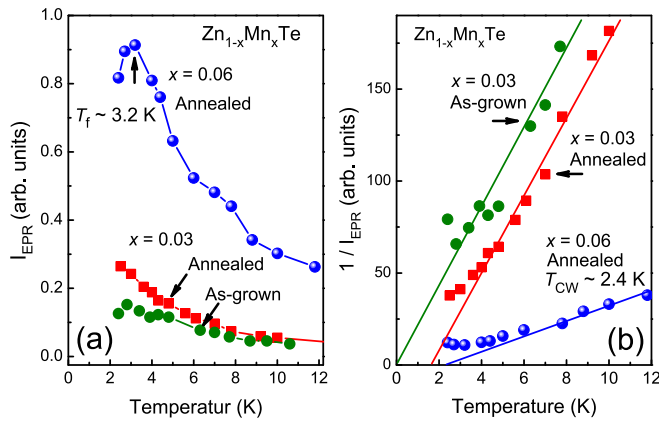


FIG. 7. (a) Temperature dependence of the EPR signal intensity I_{EPR} for as-grown and annealed samples $\text{Zn}_{0.97}\text{Mn}_{0.03}\text{Te}$, and for annealed sample $\text{Zn}_{0.94}\text{Mn}_{0.06}\text{Te}$. (b) Temperature dependence of $1/I_{\text{EPR}}$ for the same samples as in (a). Solid lines show linear fits, which serve us to determine the Curie-Weiss temperature T_{CW} .

line to Mn^{2+} ions. The measured value $g = 2.0048$ is higher than the value $g_{\text{Mn}} = 2.0$ for a single isolated Mn^{2+} ion with total spin $S = 5/2$ and total orbital momentum $L = 0$. We suggest that the Mn^{2+} - Mn^{3+} ferromagnetic double-exchange coupling may cause the enhancement of the experimental value of the Mn^{2+} g factor. The peak-to-peak amplitude and linewidth of the EPR spectrum increase with decreasing temperature, and they tend to saturate below $T = 6$ K. This indicates a strong coupling among the Mn ions. The intensity I_{EPR} is calculated by a double integration of the experimental EPR spectrum. It is established that I_{EPR} is proportional to the magnetic susceptibility χ of the Mn subsystem [17,27]. In the high-temperature limit, the temperature dependence of $I_{\text{EPR}}(T)$ can be described by [28]

$$I_{\text{EPR}}(T) = \frac{C}{T - T_{\text{CW}}}, \quad (7)$$

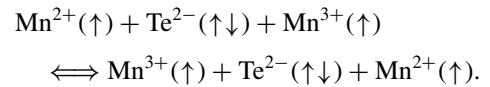
where C is the Curie constant and T_{CW} is the Curie-Weiss temperature.

Figure 7(a) presents the temperature dependence of $I_{\text{EPR}}(T)$ for the as-grown and the annealed $\text{Zn}_{0.97}\text{Mn}_{0.03}\text{Te}$ samples, and the annealed $\text{Zn}_{0.94}\text{Mn}_{0.06}\text{Te}$ sample. It is seen that at low temperatures I_{EPR} increases with decreasing temperature, following a Curie paramagnetic dependence, $1/T$. The PL measurements have revealed that annealing the $\text{Zn}_{1-x}\text{Mn}_x\text{Te}$ crystals under a high pressure of nitrogen gas increases the concentration of the V_{Zn}^- acceptors (not shown here). Correspondingly, the I_{EPR} of the annealed $\text{Zn}_{0.97}\text{Mn}_{0.03}\text{Te}$ sample increases by a factor of 1.5 in comparison to that of the as-grown sample. An important feature which can be seen from Fig. 7(a) is that $I_{\text{EPR}}(T)$ of the $\text{Zn}_{0.94}\text{Mn}_{0.06}\text{Te}$ sample exhibits a cusplike peak at $T_f \approx 3.2$ K suggesting a transition from paramagnetic to spin-glass phase. This conclusion is reached due to the fact that the transition occurs rather slowly (over 8 K); see Ref. [29]. The spin-glass phase at $T < 3.2$ K is a clear indication of the presence of the ferromagnetic interaction between Mn^{2+} and Mn^{3+} ions which competes with the intrinsic Mn^{2+} - Mn^{2+} antiferromagnetic superexchange interaction in $\text{Zn}_{1-x}\text{Mn}_x\text{Te}$. Due to

this property the Mn molar fraction ($x = 0.06$) at which the spin-glass phase occurs is much lower than the percolation threshold $x_c = 0.17$ [30,31], observed in the DMS with lattice frustration.

Figure 7(b) displays plots of the inverse of $I_{\text{EPR}}(T)$ versus temperature for the as-grown and annealed $\text{Zn}_{0.97}\text{Mn}_{0.03}\text{Te}$ sample, and for the annealed $\text{Zn}_{0.94}\text{Mn}_{0.06}\text{Te}$ sample. Solid lines show linear fits, which serve us to determine the Curie-Weiss temperature, T_{CW} . The fitting results show $T_{\text{CW}} = +1.52$ K and $+2.4$ K for the annealed $\text{Zn}_{0.97}\text{Mn}_{0.03}\text{Te}$ and $\text{Zn}_{0.94}\text{Mn}_{0.06}\text{Te}$ samples, respectively. The positive sign of T_{CW} is an indication of the presence of ferromagnetic interaction between Mn ions in the $\text{Zn}_{1-x}\text{Mn}_x\text{Te}$ samples.

Let us discuss the origin of the FM interaction in our undoped $\text{Zn}_{1-x}\text{Mn}_x\text{Te}$. It has been reported so far that in $\text{Zn}_{1-x}\text{Mn}_x\text{Te}$ doped with nitrogen (N) the ferromagnetism of the Mn subsystem is governed by the Ruderman-Kittel-Kasuya-Yosida (RKKY) interaction [32]. In this case the Mn ions are in the 2+ charge state and the hole concentration required to mediate the Mn-Mn FM interaction is about $p \approx 10^{26} \text{ m}^{-3}$. The $\text{Zn}_{1-x}\text{Mn}_x\text{Te}$ samples which we have used for the PL and EPR experiments are undoped, with the hole concentration $p \leq 10^{22} \text{ m}^{-3}$. Therefore, the observed FM interaction in these undoped samples must be caused by a mechanism other than the RKKY coupling. Based on the PL results which have shown the existence of Mn^{3+} ions in $\text{Zn}_{1-x}\text{Mn}_x\text{Te}$, we conclude that the simultaneous presence of Mn^{2+} and Mn^{3+} ions can induce local ferromagnetic double-exchange interaction [11] via the Te^{2-} ions:



We consider the positive sign of T_{CW} in the undoped $\text{Zn}_{1-x}\text{Mn}_x\text{Te}$ as an EPR indication of the presence of Mn^{3+} ions.

IV. DISCUSSION

It is established that Mn is divalent in II-VI compounds, and has a high-spin d^5 electron configuration characterized by $S = 5/2$; i.e., the individual Mn^{2+} ions are electrically inactive in the II-VI host. The experimental results reported in the present paper and in our earlier work Ref. [2] show that in $\text{Zn}_{1-x}\text{Mn}_x\text{Te}$ the interaction between Mn^{2+} ions and holes trapped at the V_{Zn}^- or phosphorus (P^{2-}) acceptors leads to the charge transfer from Mn^{2+} ions to the acceptors. As a result, the charge state of Mn^{2+} ions is changed from +2 to +3 and the efficiency of the acceptor doping of $\text{Zn}_{1-x}\text{Mn}_x\text{Te}$ is limited.

Interestingly, the change of the charge state of Mn^{2+} ions due to the charge transfer between Mn^{2+} ions and the doped acceptors has also been observed in $\text{III}_{1-x}\text{Mn}_x\text{V}$ DMSs, such as $\text{GaN}:(\text{Mn},\text{Mg})$ [33,34], $\text{GaP}:(\text{Mn},\text{Zn})$ [35], and $\text{GaAs}:(\text{Mn},\text{Be})$ [36]. In these DMSs the co-doping of Mn and acceptor impurities leads to the mixed valence of Mn, strong decrease in the Curie temperature, and creation of highly resistive materials. Therefore, the change of the charge state of Mn^{2+} ions due to their interaction with the acceptor impurities is a common property in the $\text{II}_{1-x}\text{Mn}_x\text{VI}$ and

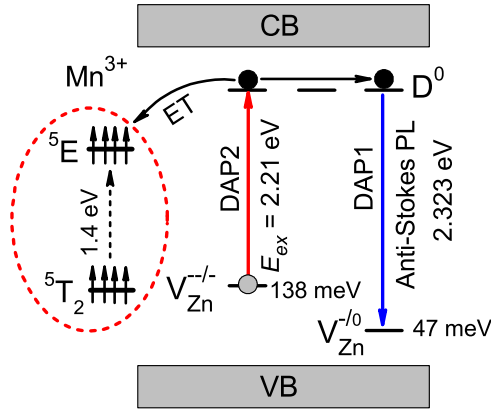


FIG. 8. Schematic illustration of the resonant excitation for the DAP2 transition that leads to the occurrence of the DAP1 anti-Stokes emission and the 1.4 eV intra-Mn³⁺ emission. The Mn³⁺ ions are represented by the spin-allowed $^5T_2 \leftrightarrow ^5E$ transition. ET denotes the energy transfer from the excited donor-deep acceptor pairs (DAP2) to Mn³⁺ ions.

III_{1-x}Mn_xV alloys. That causes a great technological problem for production of the DMS with a high Mn concentration and a high free hole density in parallel. On the other hand, this property provides a possibility to create the ferromagnetic interaction between Mn²⁺ and Mn³⁺ ions by the double exchange mechanism.

Further, the existence of the Mn²⁺ and Mn³⁺ states raises the question of where the Mn^{2+/3+} energy level resides in the band structure of Zn_{1-x}Mn_xTe. In Sec. III A, we have shown that the individual Mn²⁺ ions not pairing with V_{Zn}⁻ acceptors are electrically inactive. The Mn³⁺ ions are created by the charge transfer transitions in the Mn²⁺-V_{Zn}⁻ complexes. These transitions do not provide free holes to the valence band. Therefore, we conclude that the Mn^{2+/3+} energy level must reside in the valence band at about 3.5 eV below its maximum, as early determined by photoemission experiments [17,37–39].

Let us illustrate the mechanism of the intra-Mn³⁺ emission and anti-Stokes PL emission (DAP1 band) under the 2.21 eV (DAP2) excitation. In Fig. 8 we present a schematic energy diagram showing the resonant excitation for the DAP2 transition that results in the occurrence of the 2.321 eV DAP1 anti-Stokes emission and the 1.4 eV intra-Mn³⁺ emission. The Mn²⁺, Mn³⁺, and DAP1 PL emission spectra detected under the resonant excitation are presented in Figs. 5(a)–5(c). It is seen that even under the resonant excitation of DAP2 transition there is no PL signal due to DAP2 transition. That indicates that the DAP2-Mn³⁺ energy transfer is very efficient because the $^5T_2 \leftrightarrow ^5E$ intra-Mn³⁺ transitions are spin allowed. The anti-Stokes spin-polarized DAP1 emission occurs due to the double-acceptor nature of the V_{Zn}⁻ defects.

The important result of the present study is the revealing of the strong Mn²⁺-V_{Zn}⁻ coupling that results in the creation of Mn³⁺ ions. This allows us to interpret the origin of the infrared PL band observed in the Mn-based II-VI DMSs. In the earlier studies of the PL properties in II_{1-x}Mn_xVI DMS, it was observed that the PL spectra of the II_{1-x}Mn_xVI alloys exhibit two emission bands in parallel associated with Mn

TABLE II. Energies of the Mn²⁺ and Mn³⁺ emission bands in II_{1-x}Mn_xVI alloys.

Sample	Mn ²⁺ (eV)	Mn ³⁺ (eV)	References
Zn _{1-x} Mn _x S	2.1	1.31	[41]
Zn _{1-x} Mn _x Se	2.12	1.30	[40]
Zn _{1-x} Mn _x Te	1.96	1.44	Present work
Cd _{1-x} Mn _x S	2.15	1.37	[42]
Cd _{1-x} Mn _x Te	1.97	1.2	[43,44]
	($x \geq 0.30$)	($x \geq 0.05$)	

ions. The first is the visible PL band which peaks at ≈ 2.1 eV. This band is attributed to the Mn²⁺ intrashell transition. The second is the infrared (IR) band which peaks at ≈ 1.2 eV. The nature of the IR band is not clear till present [40,43]. Based on the results of the PL measurements presented in Sec. III B, we suggest that the 1.2 eV IR band is due to the intra-Mn³⁺ transition, $^5T_2 \rightarrow ^5E$. In Table II we summarize the energy values of the Mn²⁺ and Mn³⁺ emission bands for the II_{1-x}Mn_xVI alloys.

It is worth noting that although the ~ 2.1 eV Mn²⁺ emission has been observed for a long time and is believed to originate from the Mn²⁺ intrashell spin-forbidden transition $^4T_1 \rightarrow ^6A_1$ [17,18], the breaking of the spin selection rule for this transition has given rise to serious complications in the interpretation of the origin of this emission. During the last three decades, various models have been proposed [20,45–49] to explain the mechanisms of the $^4T_1 \rightarrow ^6A_1$ transition. According to the reported models the excitation of the Mn²⁺ ions from the 6A_1 ground state to the 4T_1 excited state is suggested to occur through one of the three excitation mechanisms, namely, the direct energy transfer from the band states (excitons) to Mn²⁺ ions [20,45], the charge transfer by the host [46,47], or the Mn²⁺-Mn²⁺ spin-flip coupling [48,49]. The third mechanism invokes an electronic transition of an excited Mn²⁺ ion to the 6A_1 ground state with the simultaneous spin flip of one of the neighboring Mn²⁺ ions.

Our PL experiments have shown that under the 2.21 eV resonant excitation the Mn²⁺ emission intensity increases by a factor of 50 in comparison to that observed under the above band gap (2.54 eV) excitation, and an anti-Stokes PL line appears at 2.32 eV (see Fig. 5). This finding shows that an individual Mn²⁺ ion which does not couple with a V_{Zn}⁻ acceptor may undergo a spin-flip interaction with a photoexcited electron trapped at a neutral donor D⁰. The Mn²⁺-D⁰ spin-flip coupling can relax spin selection rules for Mn²⁺ intrashell transitions and enables these transition to happen. This Mn²⁺ excitation/recombination processes can be described as

$$^6A_1(\pm 5/2) + D^0(\mp 1/2) \leftrightarrow ^4T_1(\pm 3/2) + D^0(\pm 1/2). \quad (8)$$

Transitions (8) are allowed if the total spin projection $S_{\text{tot}} = S_z^{\text{Mn}} + s_z^e$ of the Mn²⁺ + D⁰ system along the direction of the applied magnetic field for the initial and final states is equal to ± 2 . Here, $S_z^{\text{Mn}} = \pm 5/2$ and $s_z^e = \pm 1/2$ are the spin projections of the Mn²⁺ ion and of the electron bound to D⁰ neutral donors.

We suggest that the Mn²⁺-D⁰ spin-flip coupling is a basic mechanism of Mn²⁺ emission under the below band gap excitation. The fact that this mechanism effectively operates under the DAP2 resonant excitation, i.e., in the absence of the free band carriers, shows that the energy transfer or charge transfer mechanisms are not the main mechanisms of Mn²⁺ emission.

V. SUMMARY

We have studied the temperature dependence of free hole concentration, photoluminescence associated with Mn²⁺, Mn³⁺ ions, V_{Zn} defects, and magnetic susceptibility in the Zn_{1-x}Mn_xTe DMS. We have observed a strong interaction between Mn²⁺ ions and holes trapped at the V_{Zn}⁻ defects, resulting in the formation of the Mn²⁺-V_{Zn}⁻ charge transfer complexes. These complexes cause the transformation of the 0.047 eV V_{Zn}^{-/0} shallow acceptor level, present in ZnTe, into a 0.138 eV V_{Zn}^{-/-} deep acceptor level and induce a new 1.44 eV PL band associated with Mn³⁺ ions in Zn_{1-x}Mn_xTe. The coexistence of the mixed valence Mn²⁺ and Mn³⁺ states leads to the local ferromagnetic exchange interaction between

Mn²⁺ and Mn³⁺ ions. The competition between the ferromagnetic exchange interaction and the intrinsic Mn²⁺-Mn²⁺ antiferromagnetic superexchange coupling gives rise to the paramagnetic–spin glass phase transition at $T_f = 3.2$ K in the Zn_{1-x}Mn_xTe samples with $x = 0.06$. We suggest a charge transfer mechanism, which transforms the Mn²⁺-V_{Zn}⁻ complexes into Mn³⁺-V_{Zn}⁻ ones. We have discussed the new mechanism of Mn²⁺ emission under the donor-acceptor-pairs resonant excitation and the effect of Mn²⁺ on the p -type doping of the II-VI compounds.

ACKNOWLEDGMENTS

One of the authors (L.V.K.) would like to thank Professor P. Kossacki, Professor A. Golnik, and Dr. T. Kazimierzuk for valuable discussions and helping in photoluminescence experiments. We thank Dr. M. Górska for a critical reading of the manuscript. This work was supported in part by the Polish National Centre for Research and Development Grant No. TECHMATSTRATEG 1/346720/8/NCBR/2017.

-
- [1] Le Van Khoi, R. R. Gałazka, and W. Zawadzki, *Phys. Rev. B* **97**, 214435 (2018).
- [2] Le Van Khoi, W. Dobrowolski, T. Kazimierzuk, A. Rodek, P. Kossacki, R. R. Galazka, and W. Zawadzki, *Phys. Rev. B* **101**, 054440 (2020).
- [3] M. Aven and B. Segall, *Phys. Rev.* **130**, 81 (1963).
- [4] F. Rong and G. D. Watkins, *Phys. Rev. Lett.* **56**, 2310 (1986).
- [5] F. C. Rong, W. A. Barry, J. F. Donegan, and G. D. Watkins, *Phys. Rev. B* **54**, 7779 (1996).
- [6] J. S. Blakemore, *Solid State Physics* (W. B. Saunders Company, Philadelphia, 1970), p. 280.
- [7] F. J. Bryant and A. T. J. Baker, *Phys. Status Solidi A* **11**, 623 (1972).
- [8] R. E. Nahory and H. Y. Fan, *Phys. Rev. Lett.* **17**, 251 (1966).
- [9] G. D. Watkin, *J. Cryst. Growth* **159**, 338 (1996).
- [10] G. D. Watkin, *Phys. Rev. Lett.* **33**, 223 (1974).
- [11] C. Zener, *Phys. Rev.* **82**, 403 (1951).
- [12] G. Chen, I. Miotkowski, and A. K. Ramdas, *Phys. Rev. B* **85**, 165210 (2012).
- [13] F. J. Bryant and A. T. J. Baker, in *Luminescence in Crystals, Molecules, and Solution*, edited by F. Williams (Plenum, New York, 1973), p. 250.
- [14] T. Taguchi, S. Fujita, and Y. Inuishi, *J. Cryst. Growth* **45**, 204 (1978).
- [15] H. Mariette, R. Triboulet, and Y. Marfaing, *J. Cryst. Growth* **86**, 558 (1988).
- [16] R. Viswanatha, J. M. Pietryga, Victor I. Klimov, and S. A. Crooker, *Phys. Rev. Lett.* **107**, 067402 (2011).
- [17] J. K. Furdyna, *J. Appl. Phys.* **64**, R29 (1988).
- [18] Y. R. Lee, A. K. Ramdas, and R. L. Aggarwal, *Phys. Rev. B* **33**, 7383 (1986).
- [19] M. Skowronski, J. M. Baranowski, and L. J. Ludwicki, *Proc. Inst. Phys. Polish Akad. Sci.* **75**, 133 (1978).
- [20] M. Nawrocki, Yu. G. Rubo, J. P. Lascaray, and D. Coquillat, *Phys. Rev. B* **52**, R2241 (1995).
- [21] K. A. Baryshnikov, L. Langer, I. A. Akimov, V. L. Korenev, Yu. G. Kusrayev, N. S. Averkiev, D. R. Yakovlev, and M. Bayer, *Phys. Rev. B* **92**, 205202 (2015).
- [22] S. Marcet, D. Ferrand, D. Halley, S. Kuroda, H. Mariette, E. Gheeraert, F. J. Teran, M. L. Sadowski, R. M. Galera, and J. Cibert, *Phys. Rev. B* **74**, 125201 (2006).
- [23] J. Zenneck, T. Niermann, D. Mai, M. Roeber, M. Kocan, J. Malindretos, M. Seibt, A. Rizzi, N. Kaluza, and H. Hardtgen, *J. Appl. Phys.* **101**, 063504 (2007).
- [24] A. Wolos, A. Wyszolek, M. Kaminska, A. Twardowski, M. Bockowski, I. Grzegory, S. Porowski, and M. Potemski, *Phys. Rev. B* **70**, 245202 (2004).
- [25] P. I. Babiy, N. P. Gavaleshko, Yu. P. Gnatenko, P. A. Skubenko, and V. I. Oleinik, *Fiz. Tekh. Poluprovodn.* **12**, 2202 (1978) [*Sov. Phys. Techn. Semicond.* **12**, 2202 (1978)].
- [26] P. Jakubas and P. Bogusławski, *Phys. Rev. B* **77**, 214104 (2008).
- [27] A. Abragam and B. Bleaney, *Electron Paramagnetic Resonance of Transition Ions* (Clarendon Press, Oxford, 1970).
- [28] J. K. Furdyna and N. Samarth, *J. Appl. Phys.* **61**, 3526 (1987).
- [29] W. Dobrowolski, M. Arciszewska, B. Brodowska, V. Domukhovski, V. K. Dugaev, A. Grzęda, I. Kuryliszyn-Kudelska, M. Wójcik, and E. I. Slynko, *Sci. Sintering* **38**, 109 (2006).
- [30] A. R. Alcantara, S. Barrett, D. Matev, I. Miotkowski, A. K. Ramdas, T. M. Pekarek, and J. T. Haraldsen, *Phys. Rev. B* **104**, 104423 (2021).
- [31] R. R. Gałazka, S. Nagata, and P. H. Keesom, *Phys. Rev. B* **22**, 3344 (1980).
- [32] D. Ferrand, J. Cibert, A. Wasiela, C. Bourgoignon, S. Tatarenko, G. Fishman, T. Andrearczyk, J. Jaroszyński, S. Koleśnik, T. Dietl, B. Barbara, and D. Dufeu, *Phys. Rev. B* **63**, 085201 (2001).

- [33] T. Devillers, M. Rovezzi, N. Gonzalez Szwacki, S. Dobkowska, W. Stefanowicz, D. Sztenkiel, A. Grois, J. Suffczynski, A. Navarro-Quezada, B. Faina, T. Li, P. Glatzel, F. d'Acapito, R. Jakiela, M. Sawicki, J. A. Majewski, T. Dietl, and A. Bonanni, *Sci. Rep.* **2**, 722 (2012).
- [34] A. Wolos, M. Palczewska, M. Zajac, J. Gosk, M. Kaminska, A. Twardowski, M. Bockowski, I. Grzegory, and S. Porowski, *Phys. Rev. B* **69**, 115210 (2004).
- [35] C. Xu, Y. Yuan, M. Wanga, H. Hentschel, R. Bottger, M. Helm, and S. Zhou, *J. Magn. Magn. Mater.* **459**, 102 (2018).
- [36] S. Lee, S. J. Chung, I. S. Choi, W. L. Lim, Y. Sasaki, X. Liu, T. Wojtowicz, and J. K. Furdyna, *J. Appl. Phys.* **93**, 8307 (2003).
- [37] T. Dietl, *Semicond. Sci. Technol.* **17**, 377 (2002).
- [38] M. Taniguchi, L. Ley, R. L. Johnson, J. Ghijsen, and M. Cardona, *Phys. Rev. B* **33**, 1206 (1986).
- [39] C. Webb, M. Kaminska, M. Lichtensteiger, and J. Lagowski, *Solid State Commun.* **40**, 609 (1981).
- [40] H. Waldmann, C. Benecke, W. Brusa, H. E. Gumlich, and A. Krost, *Semicond. Sci. Technol.* **4**, 71 (1989).
- [41] C. Benecke, W. Brusa, H. E. Gumlich, and H. J. Moros, *Phys. Status Solidi B* **142**, 301 (1987).
- [42] C. Ehrlich, W. Brusa, H. E. Gumlich, and D. Tschierse, *J. Cryst. Growth* **72**, 371 (1985).
- [43] M. P. Vecchi, W. Giriat, and L. Videla, *Appl. Phys. Lett.* **38**, 99 (1981).
- [44] G. Ambrazevičius, G. Babonas, and Y. V. Rud, *Phys. Status Solidi B* **125**, 759 (1984).
- [45] H. Falk, J. Hubner, P. J. Klar, and W. Heimbrod, *Phys. Rev. B* **68**, 165203 (2003).
- [46] K. R. Pradeep and R. Viswanatha, *APL Mater.* **8**, 020901 (2020).
- [47] K. Gahlot, K. R. Pradeep, A. Camellini, G. Sirigu, G. Cerullo, M. Zavelani-Rossi, A. Singh, U. V. Waghmare, R. Viswanatha, *ACS Energy Lett.* **4**, 729 (2019).
- [48] J. F. MacKay, W. M. Becker, J. Spalek, and U. Debska, *Phys. Rev. B* **42**, 1743 (1990).
- [49] L. Dai, A. Torche, C. Strelow, T. Kipp, T. H. Vuong, J. Rabeah, K. Oldenburg, G. Bester, A. Mews, C. Klinke, and R. Lesyuk, *ACS Appl. Mater. Interfaces* **14**, 18806 (2022).